

3.1 Satellite image processing

1. Akjoujt LANDSAT image processing

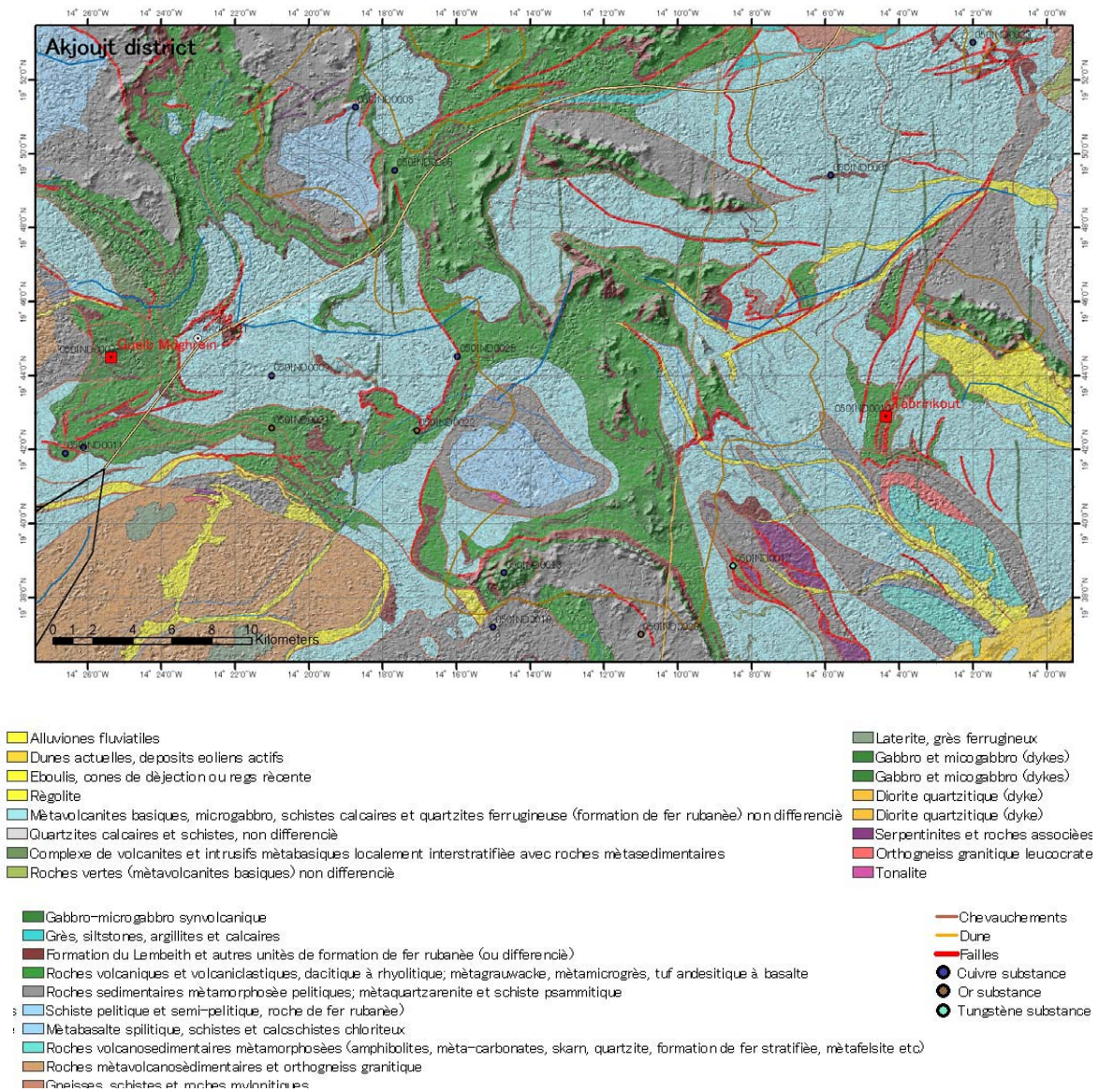


Figure 1 Geology map of the Akjoujt area (after 1:200,000 series, SIGM database)

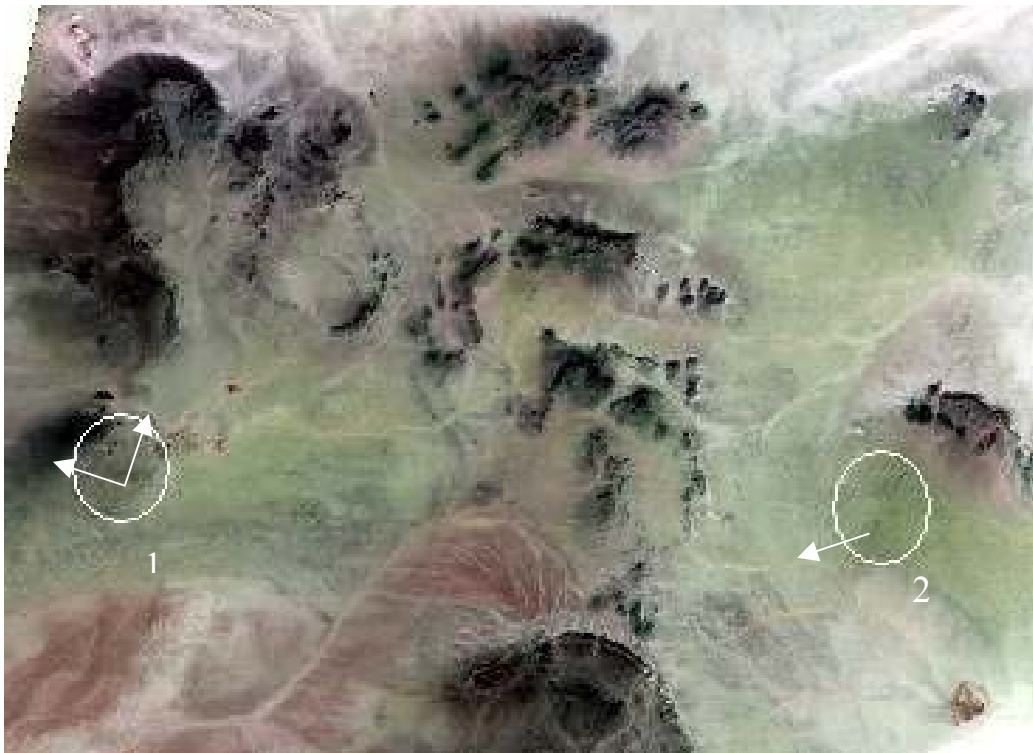


Figure 2 LANDSAT ETM Infra-red image: vegetation shows as red-pink. Area 1 = Akjoujt Cu-Au Mine; 2 = Tabrinkout tungsten anomaly. Arrows show look-direction of photos below.



Figure 3 Akjoujt Mine: looking west from residual hill / gossan, along the strike of the mineralised metacarbonate and main shear zones.



Figure 4 View north from mine towards Akjoujt hills, treatment plant, tailings dam pond and town reservoir in middle distance.



Figure 5 Looking SW from the meta-carbonate of the Tabrinkout tungsten anomaly (view along old sample trench)

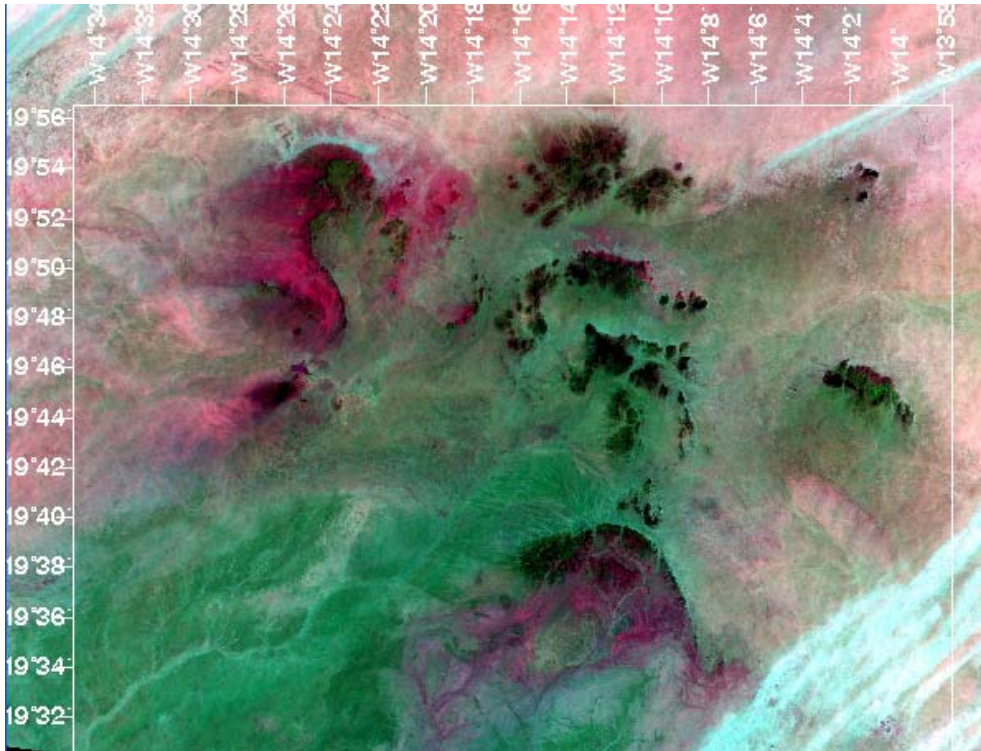


Figure 6 LANDSAT TM_731_RGB Pink = granite/migmatite;
 White-blue = quartz-rich; dark brown-ruby red = BIF & debris
 Green = schists & meta-carbonates

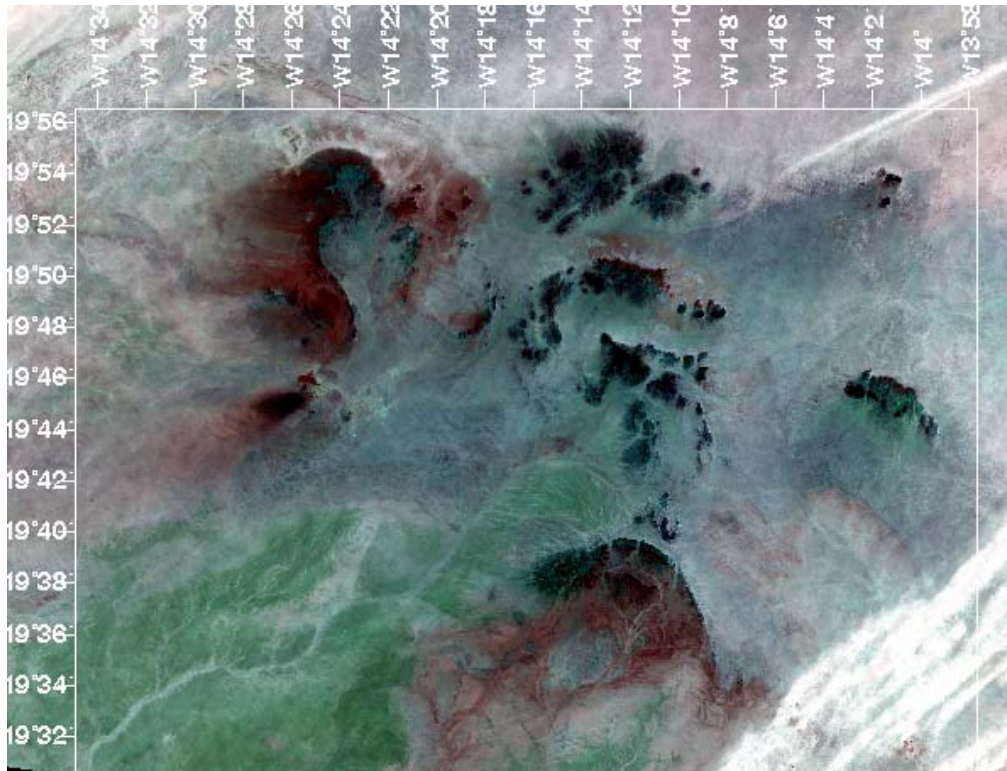


Figure 7 LANDSAT TM_(351)(517)(741)_RGB Pale blue = chlorite schists, dark grey lenses within the chlorite schists are meta-carbonates. Green in SW corner = orthogneiss?

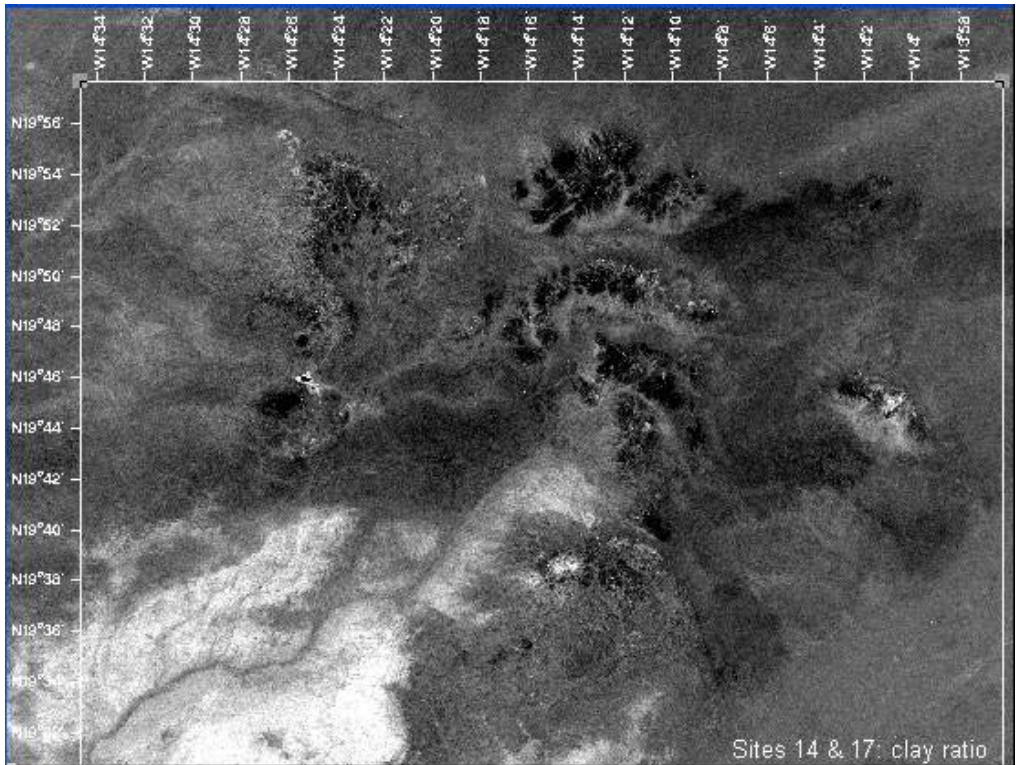


Figure 8 Clay abundance: white = maximum. No clay alteration around the Tabrinkout W anomaly; small patches of alteration around Akjoujt mine.

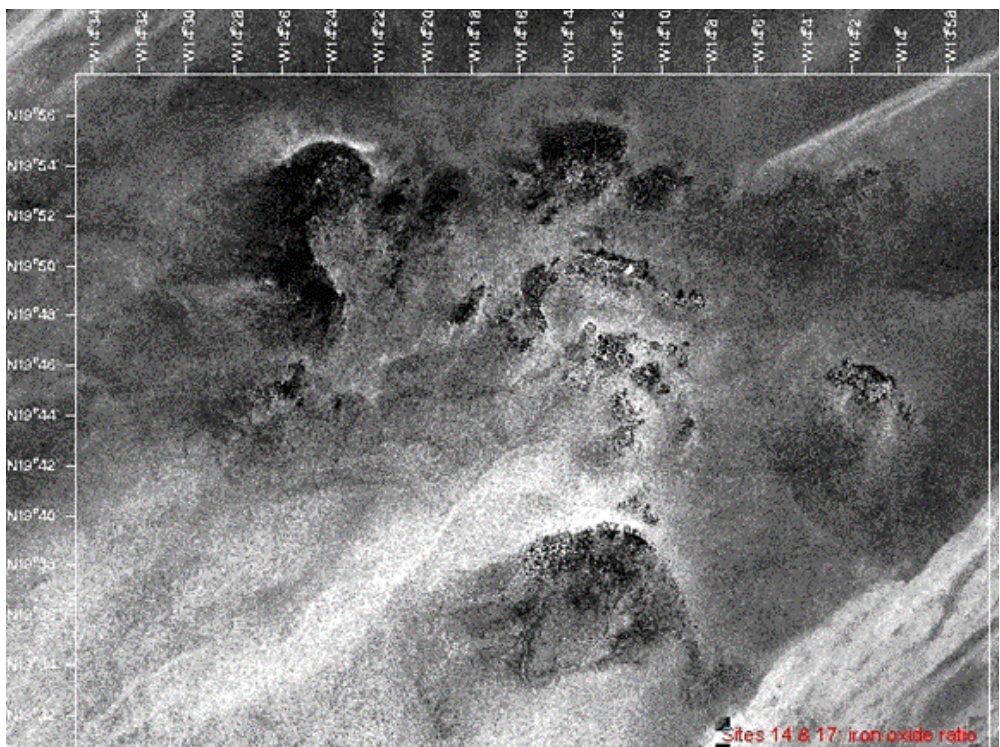


Figure 9 Fe ratio, highlighting haematite-stained dune sands and Fe-rich alluvial-colluvial sediments derived from the Banded Iron Formations, which have a speckled appearance.

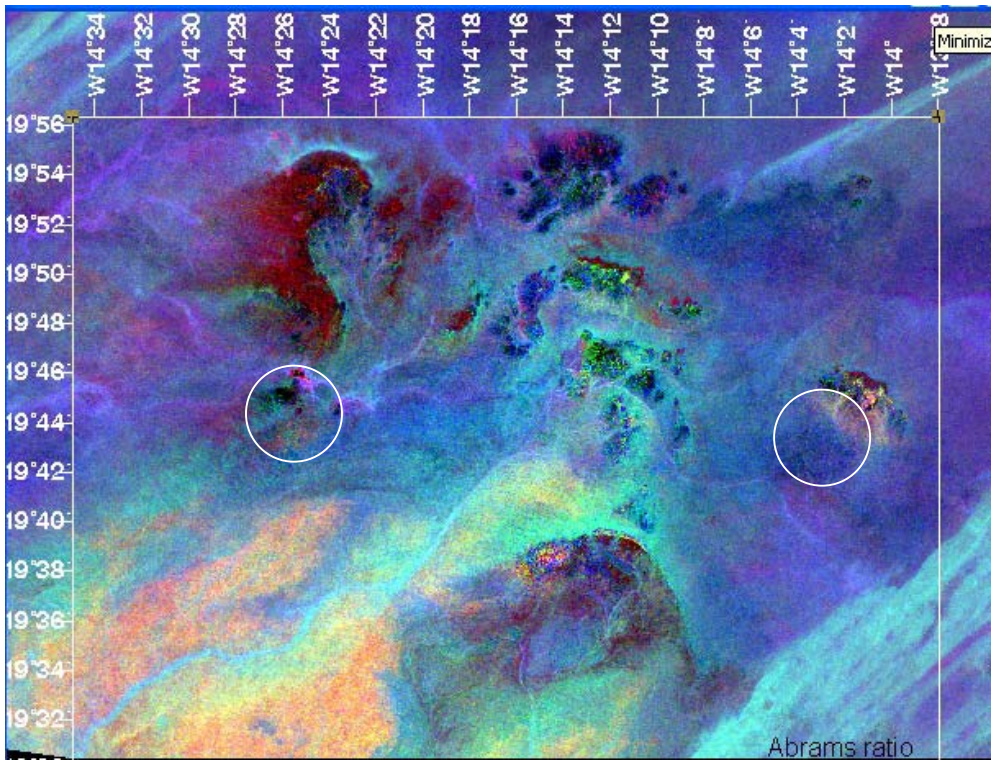


Figure 10 Abrams Ratio: clay and iron oxide abundance. Brown = hematite; yellow-red = kaolinite and iron oxides, mostly over orthogneiss; pale blue = quartz-rich; blue = schists and meta-carbonates.

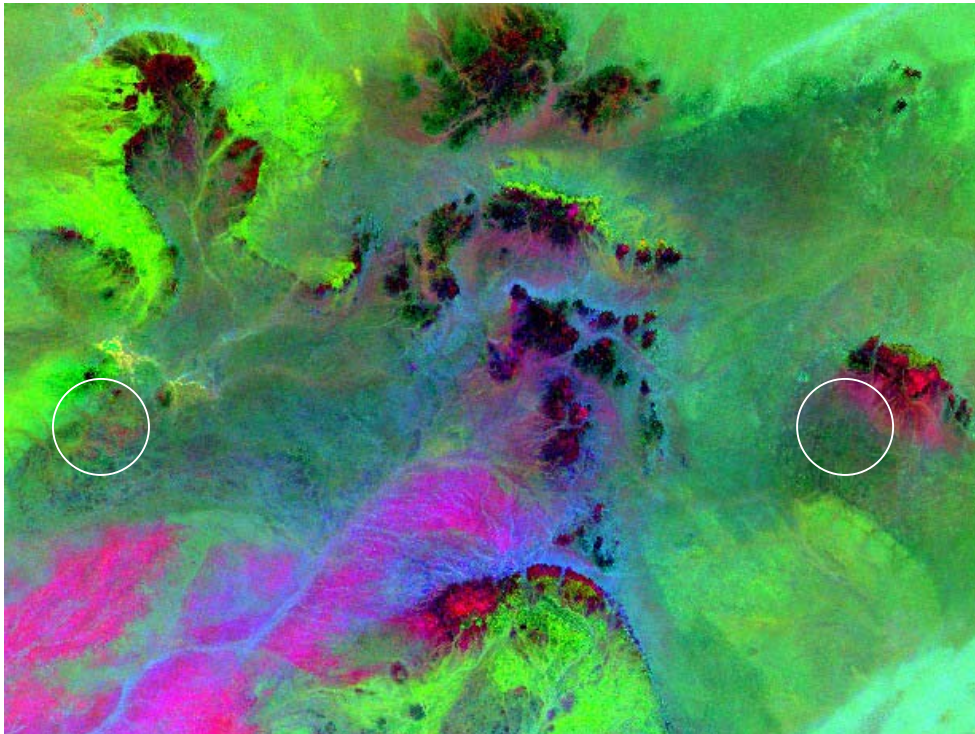


Figure 11 Complex Band Ratio ((5/7 4/5 3/1 RGB). Black-Red = BIF Pink = quartzite/orthogneiss; Dark green = chlorite schist, with dark grey lenses of meta-carbonate; grey = quartz-rich.

2. Zoueratet LANDSAT image processing

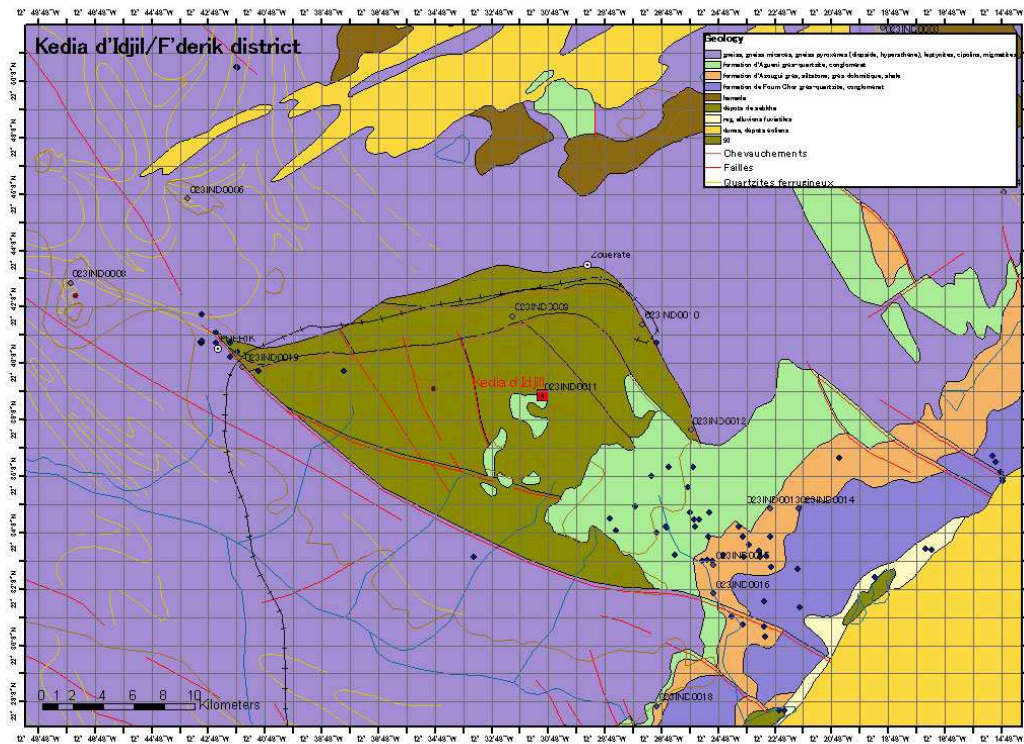


Figure 12 Geology of the F'Derik— Koedia -Idjill area (after 1:200,000 series, SIGM database)

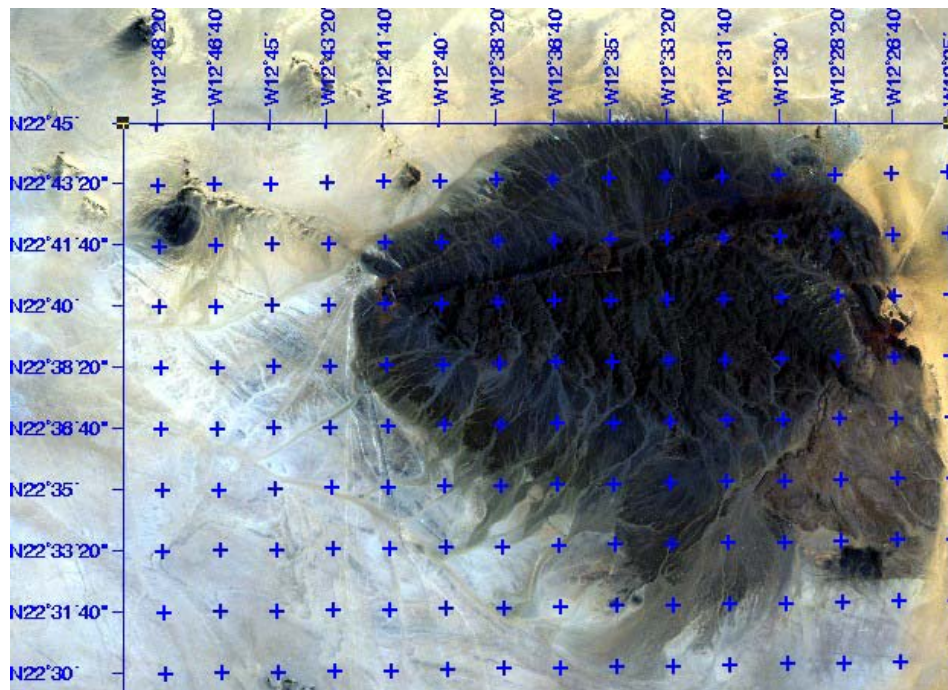


Figure 13 LANDSAT ETM false-colour infra-red image (432 RGB)

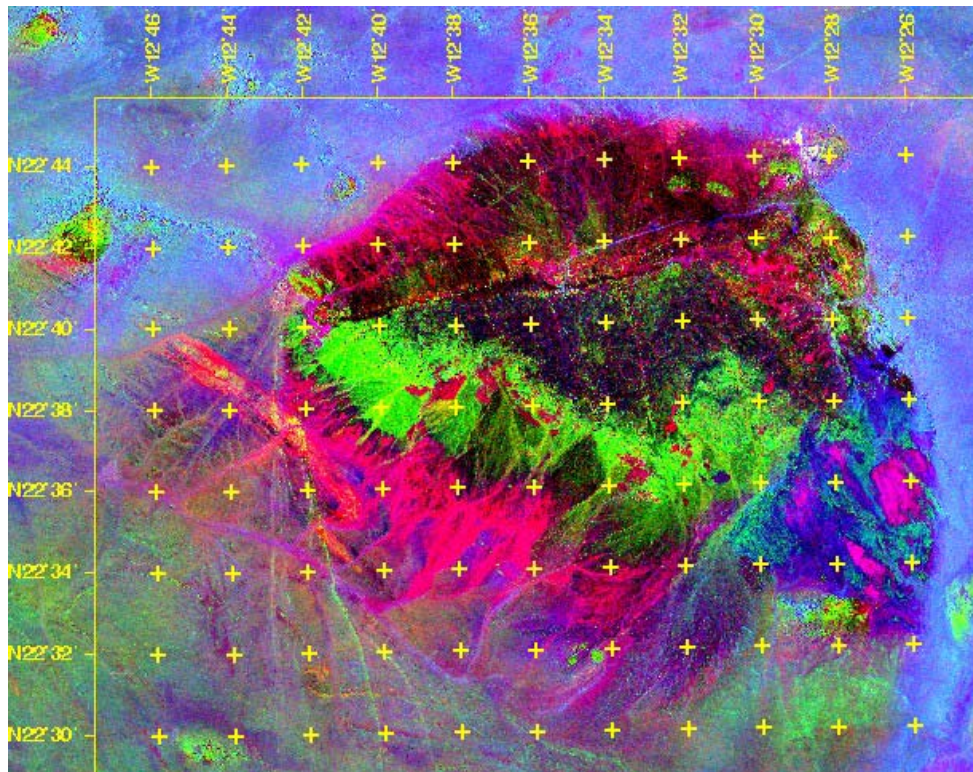


Figure 14 LANDSAT ETM: 5/7 4/3 3/1 RGB. Red-black = iron oxides / laterite
Green = iron hydroxides; Blue = quartz-rich; Pink-blue = conglomerate.

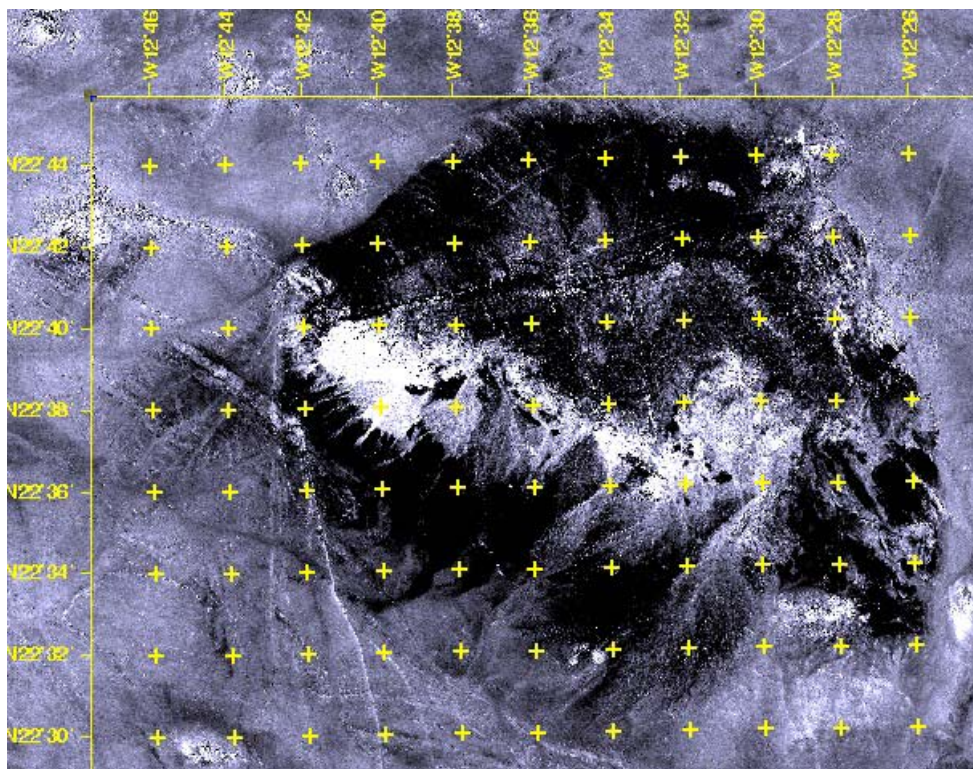


Figure 15 LANDSAT ETM 5/4 – abundance of iron hydroxides (white)

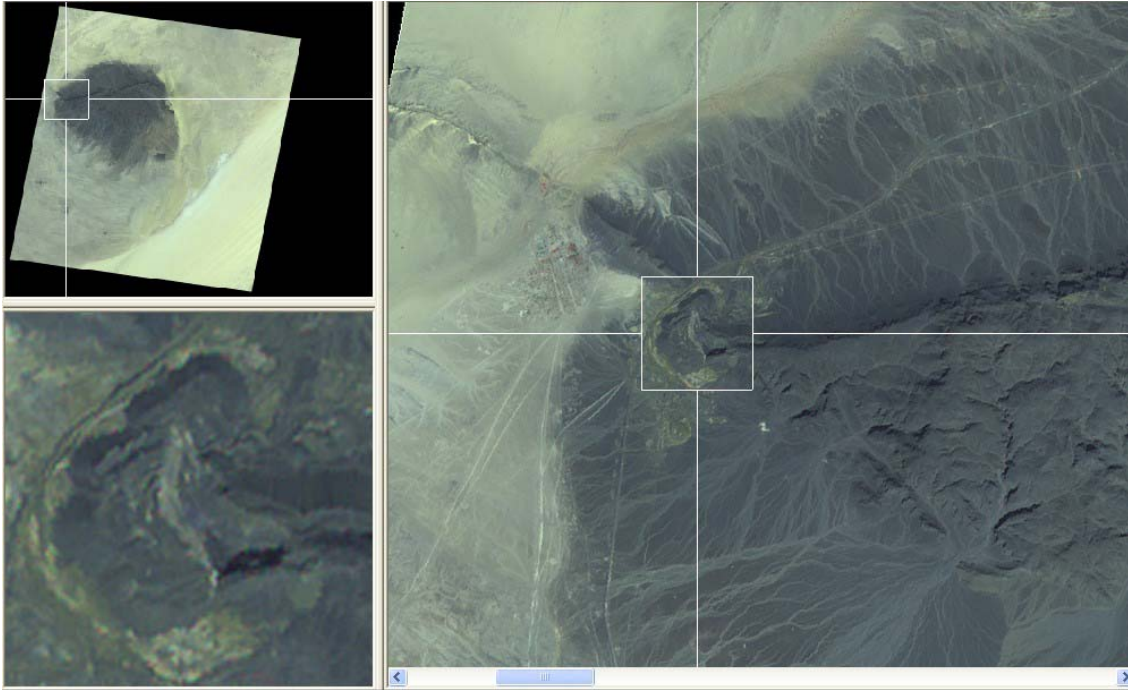


Figure 16 ASTER false-colour infra-red (321 RGB), focused on F'Derik Fe Mine.

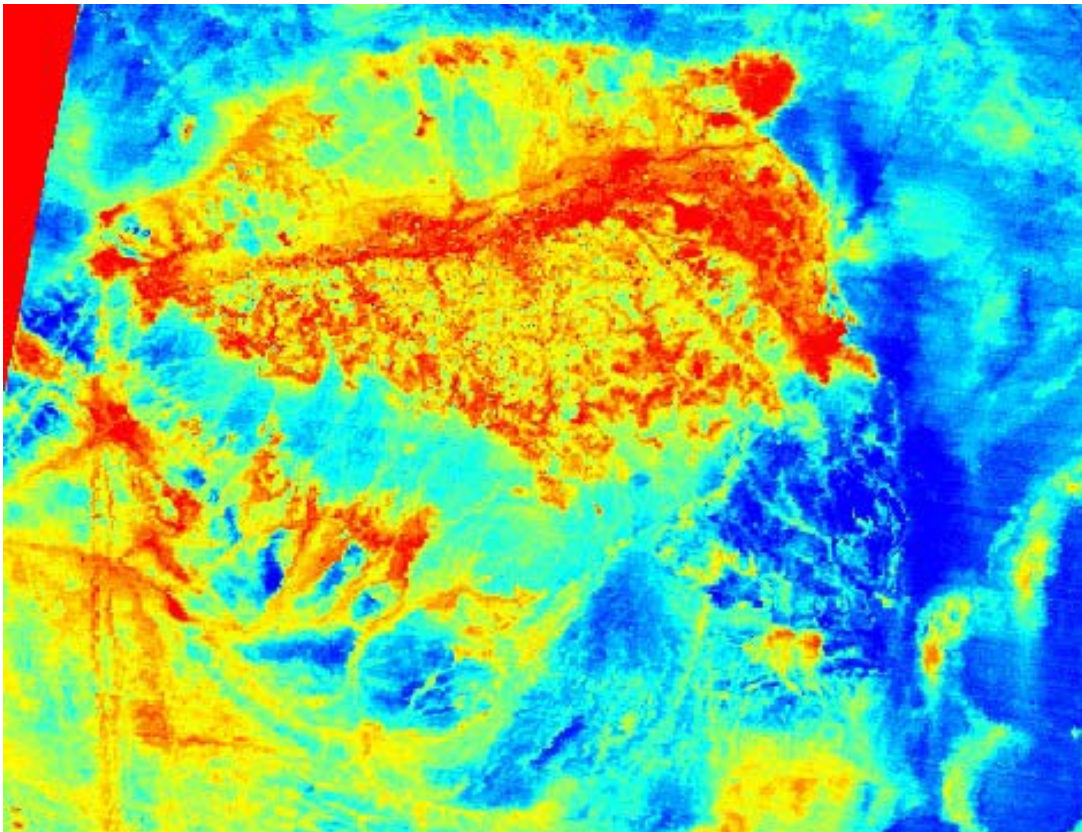


Figure 17 ASTER thermal band ratio (13/14)

3. Tasiast LANDSAT image processing

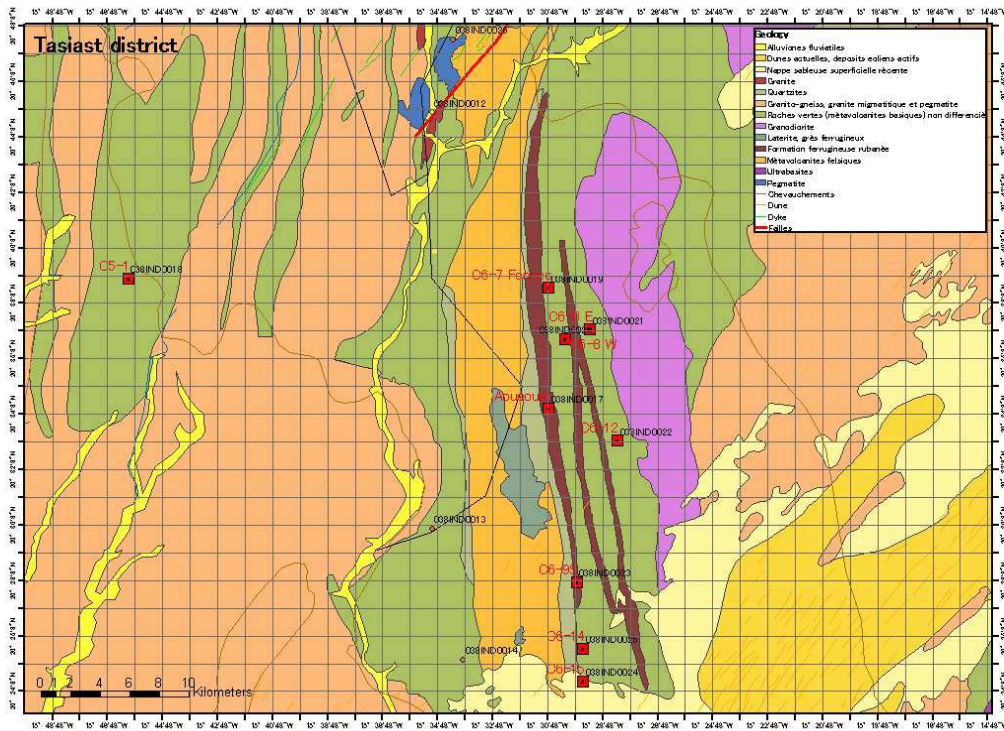


Figure 18 Geological map of Tasiast area (after 1:200,000 series, SIGM database)

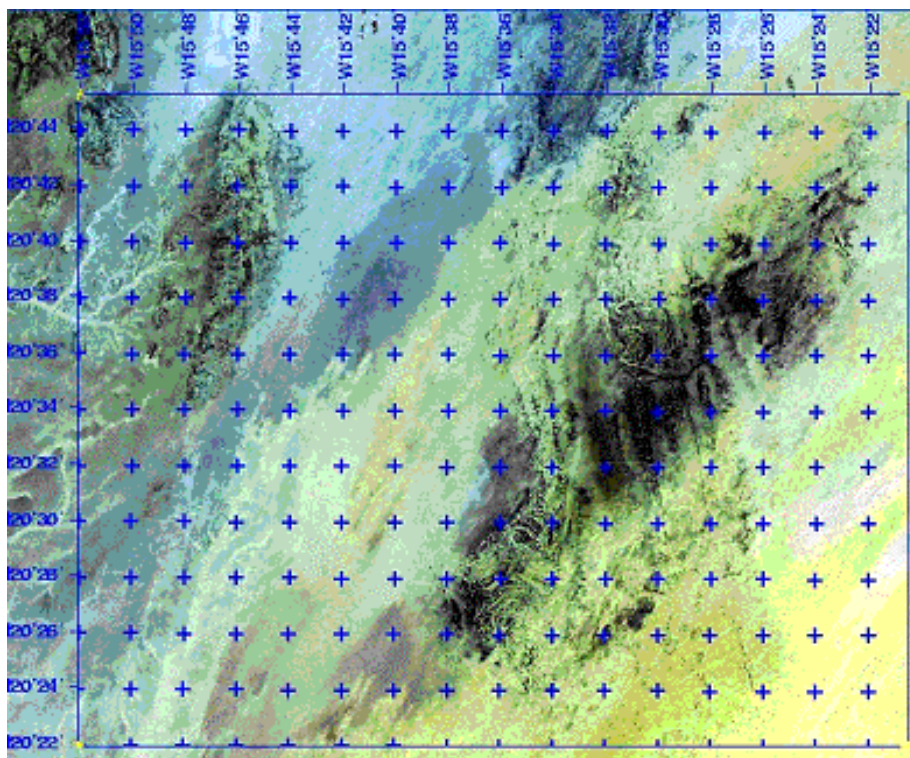


Figure 19 LANDSAT ETM 'true-colour' image of Tasiast (321 RGB)

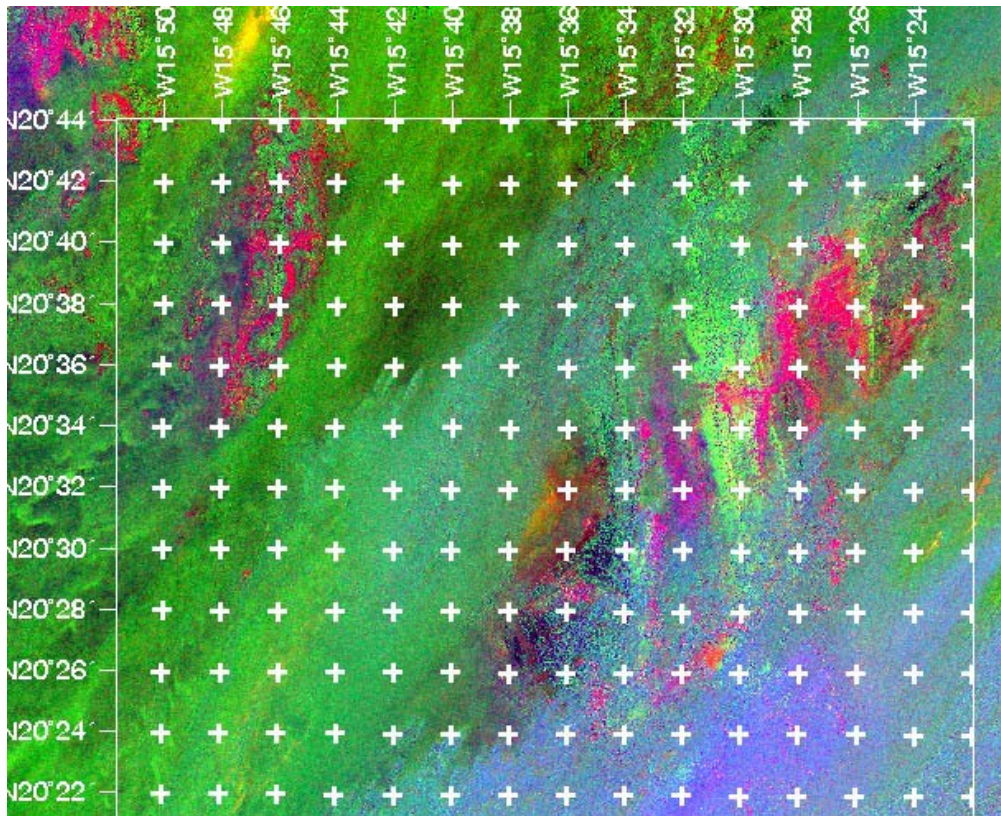


Figure 20 Tasiast - LANDSAT ETM 5/7 4/5 3/1 RGB. Dark Green = migmatite/gneiss; Blue = quartz-rich; Blue-Pink = felsic metavolcanics; Apple Green = granite; Red = Granodiorite; Red-Brown = Greenstone Belt laterite.

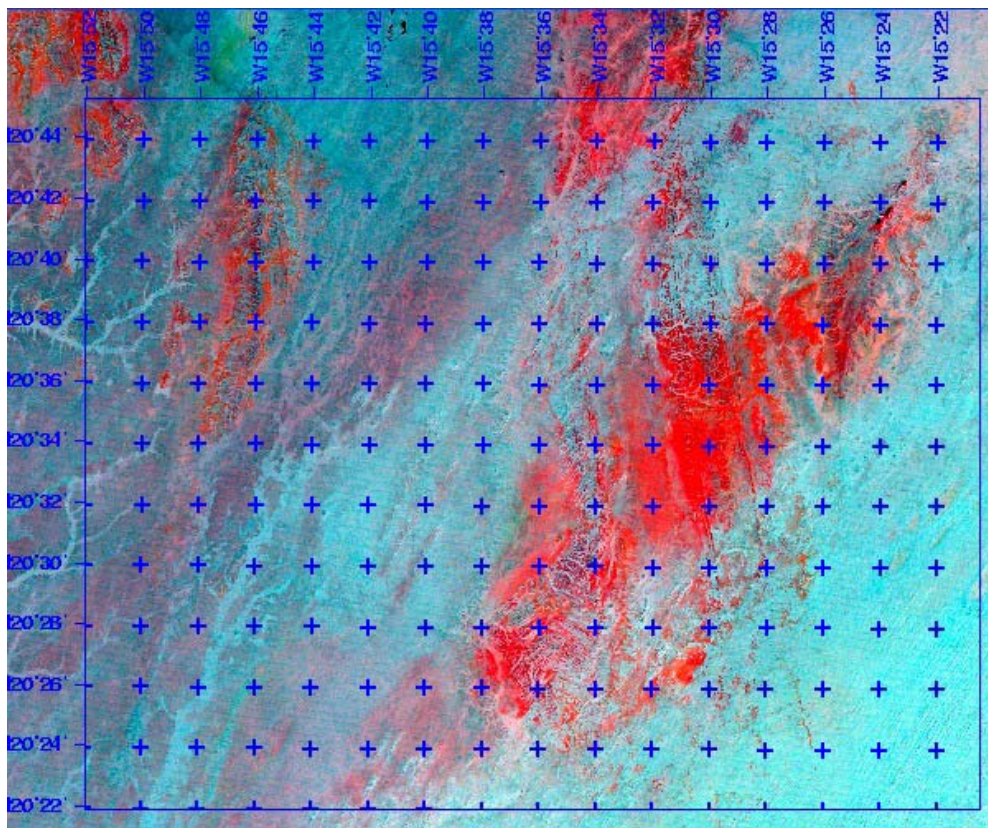


Figure 21 Tasiast – LANDSAT 657 RGB – thermal anomalies in red.

3.2 Remote sensing analysis

1. The Role of Remote Sensing Analysis for Mineral Resources Survey

The role of remote sensing for mineral resources survey means analysis of geological structure and grasping of location and size of mineral resources. Mineral resources survey is divided into each stages of general survey, detailed survey, prospecting drilling and mining exploitation. It is used for remote sensing to select high potential area of prospecting in general surveying stage, extract drilling area in detailed surveying stage, to survey neighboring area of mineral deposit in the prospecting drilling stage, to monitor effect of mining and drain water in mining exploitation stage.

The practicable surface depth by remote sensing analysis corresponds to few micrometers from surface in the case of optical sensor, maximum 10 meter in the case of radar. As the reason of metallic ore deposit is able to appear relatively shallow place underground, it is useful for remote sensing as direct prospecting method.

Mainly, remote sensing analysis is separated to classification of rock or mineral and analysis of geological structure. Reflectance and radiant spectral of rock and mineral using optical sensor is the information reflected chemical composition of mineral. The other, the information using radar shows roughness of ground surface.

Porphyry copper deposit and shallow water-based gold deposit accompany with some extent alteration zone on ground surface. Remote sensing using optical sensor is useful for mineral investigation to grasp the distribution of alteration mineral. In recent years, hyper spectral resolution sensor, which has few of ten to few hundred-observation bands, put to practical use. The sensor can recognize and identify mineral.

2. Data for Remote Sensing Analysis

As for the data for remote sensing analysis, they are an observed spectrum, and information on the topographical features by the sensor carried on the satellite or the airplane. This time, it made use of satellite data because surveying period was short and survey area was vast. At present, the satellite data, which are the most effective in the mineral resources survey, are LANDSAT of the United States and an ASTER satellite by the Japanese-American cooperation.

Many data are accumulated since LANDSAT is launched by the United States as a global resources satellite in 1972. After 1984 years, 2.2 μ m (band 7) of the short infrared wavelength was added in the LANDSAT satellite with request of the resources survey user. This band, which is called Clay Band, is made effective in resources survey because it shows absorption of various clay minerals, carbonic acid salt mineral, and so on. ASTER (Advanced Space-borne Thermal Emission and Reflection) is the global resources satellite where it is launched in 1999. ASTER observes into each five bands which are infrared bands(8.125~11.65 μ m) and thermal infrared bands (2.0~2.5 μ m), so that it can precisely recognize mineral survey.

Table 2.1 shows the comparison of LANDSAT and ASTER data. The main differences are the

ground resolution and the number of observation bands. In this study ASTER data are mainly used and LANDSAT data are complemented. In the appendix, satellite data list and coverage map of satellite are shown.

Table 2.1 Comparison of LANDSAT and ASTER data

| Term | LANDSAT ETM | | | | ASTER | | | |
|------------------|----------------------------------|-------|------------|---------------------------|-------------------------|-------------|-------------|------------|
| Band number | 8bands(Band 8:Panchromatic mode) | | | | 14 bands (except DEM) | | | |
| Wavelength | | | | Unit (μm) | | | | Unit (μm) |
| | Visible | Blue | Band1 | 0.45 ~0.52 | VNIR | Green | Band1 | 0.52 ~0.60 |
| | | Green | Band2 | 0.53 ~0.61 | | Red | Band2 | 0.63 ~0.69 |
| | | Red | Band3 | 0.63 ~0.69 | | | | |
| | Near infrared | | Band4 | 0.75 ~0.90 | SWIR (Near infrared) | Band3 | 0.76 ~0.86 | |
| | | | Band5 | 1.55 ~1.75 | | Band4 | 1.600~1.700 | |
| | | | Band7 | 2.09 ~2.35 | | Band5 | 2.145~2.185 | |
| | | | | Band6 | | 2.185~2.225 | | |
| | | | | Band7 | | 2.235~2.285 | | |
| Thermal Infrared | | Band6 | 10.4~12.5 | TIR (Thermal Infrared) | Band8 | 2.295~2.365 | | |
| | | | | | Band9 | 2.360~2.430 | | |
| | | | | | Band10 | 8.125~8.475 | | |
| | | | | | Band11 | 8.475~8.825 | | |
| Panchromatic | | Band8 | 0.52 ~0.90 | | | | | |
| | | | | | | | | |
| Resolution | Band1~5, 7 | | | 30m | VNIR | | | 15m |
| | Bnad6 | | | 60m | SWIR | | | 30m |
| | Band8 | | | 15m | TIR | | | 90m |

3. The Spectral Characteristic of Rock and Mineral

The various minerals composed of the rock show a spectral absorption characteristic from visible band to thermal infrared band. As remote sensing analysis is enforced to use such a mineral spectral absorption characteristic, it can recognize and identify the material distributed on the surface of the earth (Fig. 3.1). The curve in this figure is refracted downward because incidence energy of the material is absorbed selectively. Generally such a characteristic is called spectral absorption.

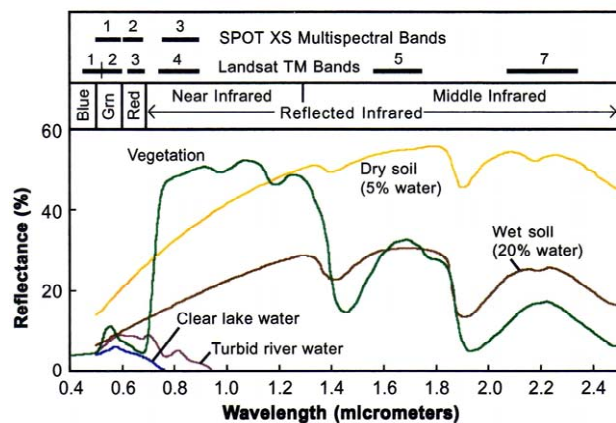


Fig. 3.1 Spectral Curve of Main Earth Surface Material. The curve in this figure is refracted downward because incidence energy of the material is absorbed selectively. Generally such a characteristic is called spectral absorption. A mineral spectral absorption characteristic shows that the wavelength, which it appears in due to physics phenomenon, is different. The shape of the spectral curve and the existence of the clear absorption region or place are decided in case of a mineral by the chemical formation and the crystal

structure. The absorption of the specific wavelength occurs due to the existence of the chemical elements and the ion, the ionization elements and the existence of the chemical bond of the elements controlled by the crystal structure. The reflection spectral curve of the typical mineral is shown in Fig.3.2.

As for the spectrum of hematite, intense absorption happens in the visible band by the iron ion. It appears that absorption range continuously between 1.8~2.4 μm in case of the calcite, which is the main element of the limestone, by existence of carbonic acid ion. Kaolinite and montmorillonite are the clay minerals contained in the soil. The absorption range, which is resistant around 1.4 μm , is shown with both as well. The absorption, which is poor around 1.9 μm , appears in case as kaolinite due to the existence of the hydroxide ion and. in case of montmorillonite, by the molecule of the interstitial water. On the other hand, remarkable absorption is not recognized as the orthoclase from the visible range to the middle infrared band.

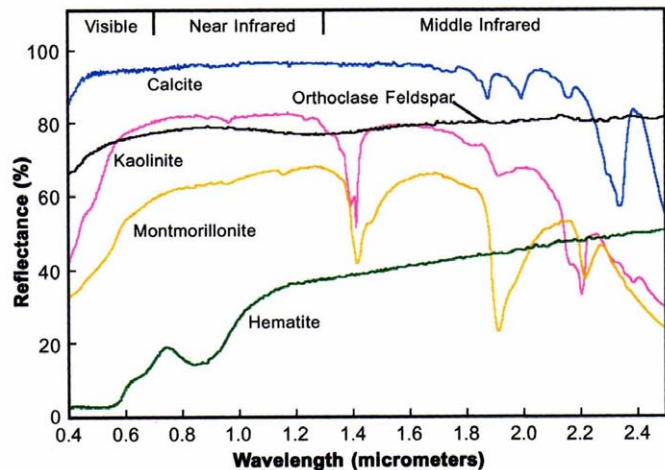


Fig. 3.2 Reflection of Spectral Curve of typical Minerals

The more detailed spectral characteristic of each bands which is divided visible band (0.4 μm ~1.0 μm), short wavelength infrared band(1.0 μm ~3.0 μm) and thermal infrared band(7.0 μm ~15.0 μm) is shown as follows.

(1) Visible band-near infrared band (0.4 μm ~1.0 μm)

The succession metal such as Fe, Mn, Cu, Ni and Cr has the spectrum caused by the transition of the electronic energy level. The reflection spectrum of the iron oxide is shown in Fig.3.3. The most remarkable absorption in the visible to near infrared band (0.4 μm ~1.0 μm) depends on charge movement between Fe-0. The reflectance of the iron oxide decreases rapidly from the blue range to ultraviolet range. The third iron absorption spectrum appears in 0.35 μm , 0.45 μm , 0.55~0.65 μm and 0.75~0.95 μm . The second iron absorption spectrum appears in 1.0~1.1 μm and 1.8~2.0 μm . Typical mineral reflection spectral curve of visible to infrared band is shown in Fig.3.4 as well.

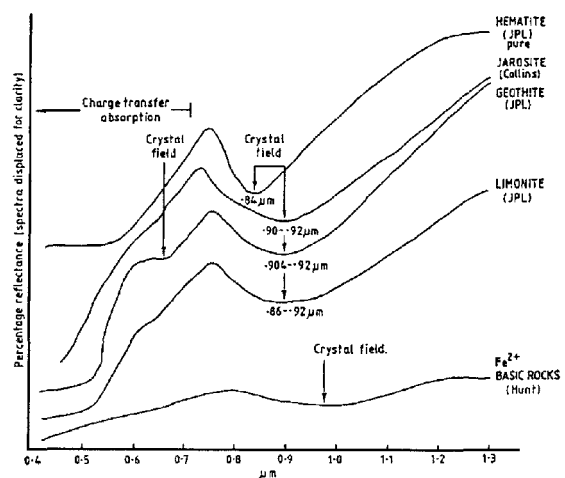


Fig. 3.4 Iron Oxide in Visible to Infrared Band

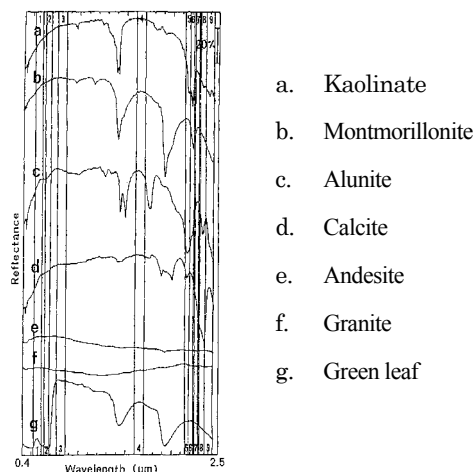


Fig.3.4 Typical mineral reflection spectral curve of visible to infrared band
(A number 1 - 9 show the observation band of ASTER).

(2) Near Infrared wavelength (1.0μm~3.0μm)

As for the short infrared wavelength, the spectrum that influences vibration between the atoms, which they combined with each other, is observed. The spectrum of the vibration of combined atom appears in 2.7μm~3.0μm and 9.0μm~11.0μm. As for these spectrum characteristics, a hydroxyl, carbonic acid base, and so on influence it in the mineral component. Especially various spectra such as a clay mineral (It has an Al-OH base, a Mg-OH base, and so on.) and carbonate mineral are important.

The main element of the clay mineral resolves due to weathering of the mother rock and hydrothermal process. The material dissolved in water such as Ca and Na is leached as that result. Si and Al, Mg and Fe that it remain, are combined with water, and it forms hydro silicate material. Some of the clay minerals (in such cases as non-crystalline silicate minerals etc.) are not layer silicate minerals, but chemical composition and crystal structure are closely related to kaolin mineral and so on, which are layer-silicate minerals.

The spectral curve of the clay mineral and carbonate mineral are shown in Fig. 3.5, and Table 3.1 shows classification of mineral for near infrared wavelength. The characteristics of the spectral reflection of clay mineral and carbonate mineral are as the following.

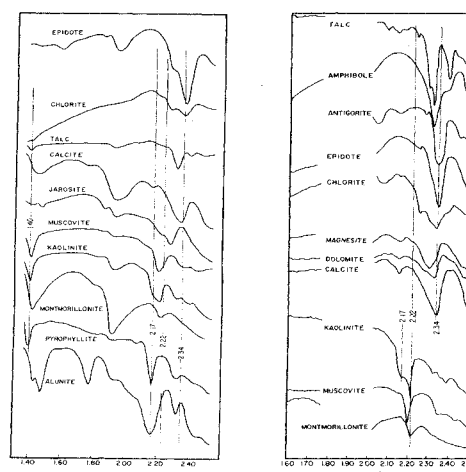


Fig. 3.5
Various Reflection Spectrum Curves of the Short Infrared Wavelength Range of the Clay and Carbonate Mineral

- a. An absorption spectrum by the Al-OH base appears in the wavelength range of 2.16~2.24 μm . Typical minerals are clay mineral and alteration mineral such as alunite, kaolinite, montmorillonite, pyrophyllite, white mica and illite. It thinks that the acid hydrothermal water, which forms alteration zone, raise with reacting with the rock and are neutralized gradually. Therefore the circulatory system of hydrothermal water is observed that zoning distribution of alteration mineral change of acidity of hypothermal corresponding to the change of acid content of hypothermal (silification rock \rightarrow alunite \rightarrow kaolinite \rightarrow montmorillonite \rightarrow propylite from the center).
- b. An absorption spectrum by the CO_3 base appears in 2.3~2.39 μm . There are various carbonate minerals such as calcite and dolomite in the mineral, which contains a CO_3 base.
- c. The absorption spectrum by the Mg-OH base appears in 2.3~2.39 μm . Typical mineral is in such cases as serpentine, the chlorite (three-octahedron), amphibole and blue site.
- d. The absorption spectrum by the Fe-OH base appears in 2.24~2.27 μm . There are jarosite, nontronite and so on in the mineral, which the characteristics of the spectrum by the Fe-OH base are shown in.

Table 3.1 Classification of Mineral for Near Infrared Wavelength

| Chemical Composition | Absorption Characteristic of Wavelength (μm) | Group of mineral | Representative mineral |
|----------------------|---|---------------------------------|--|
| Al-OH | 2.16~2.24 | Alunite | Alunite |
| | | Kaolin mineral | Kaolinite, Tychite |
| | | Pyrophyllite | Pyrophyllite |
| | | Di octahedral smectite | Montmorillonite |
| | | Di octahedral vermiculite | Vermiculite |
| | | Di octahedral mica | Mica, Illite Crystallite |
| | | Chlorite | Cokeite |
| | | Hydro oxide minerals | Gibbsite |
| | Alumino silicate minerals | Sillimanite, Topaz | |
| | 2.3~2.39 | Epidote | Epidote |
| Mg-OH | 2.3~2.39 | Serpentine | Chrysotile, Antigorite |
| | | Talc | Talc |
| | | Tri octahedral smectite | Saponite, Pectolite |
| | | Tri octahedral vermiculite | |
| | | Tri octahedral mica | Biotite, Phlogopite, Clintonite |
| | | Tri octahedral Chlorite | Chlorite |
| | | Hydro oxide minerals | Brucite |
| Amphibolite | Anthophyllite, Tremolite, Forblende | | |
| Fe-OH | 2.24~2.27 | Alunite | Jarosite |
| | | Di octahedral smectite | Nontronite |
| Si-OH | 2.24 | Water content silicate minerals | Opal |
| CO_3 | 2.3~2.39 | Carbonate minerals | Calcite, Dolomite, Siderite, Magnesite |
| H_2O | 2.0~2.5 | Salphate minerals | Gypsum |
| | | Zeolite | Natrolite, Heulandite, Anacite |

(3) Thermal infrared band (7.0 μm ~15.0 μm)

Thermal infrared wavelength range is the wavelength range which thermal radiation from ground

surface correspond the source of radiation. The spectrum, which influences a vibration between the atoms that they combined with each other, is observed in this wavelength range. The characteristic spectrum of main rock mineral is shown about the silicate mineral such as quartz, feldspar and so on in this wavelength stage.

The most important things in a mineral to distinguish in thermal infrared wavelength range are various silicate minerals. The various transparent spectrum curves of the silicate mineral are shown in the Fig.3.6 in thermal infrared wavelength range. The transparent spectral characteristic in the thermal infrared range of the typical rock is shown in the Fig.3.7.

Spectral characteristic of the silicate mineral in thermal infrared wavelength range is put together as follows.

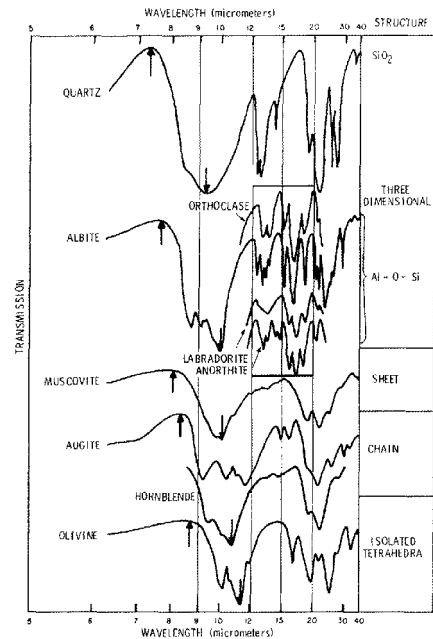


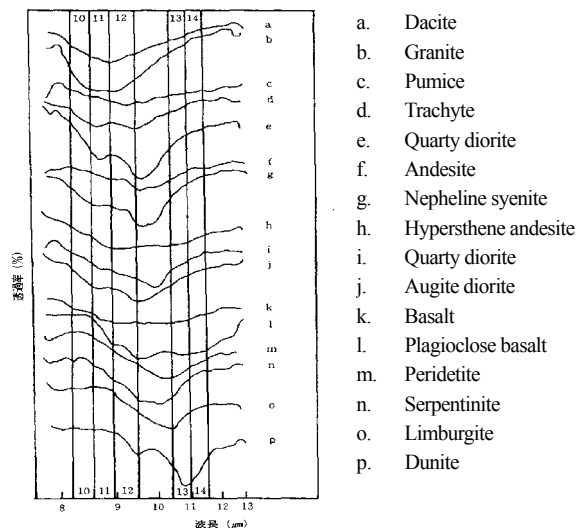
Fig. 3.6 Transparent Spectrum Curve of Silicate

- As SiO_2 content decreases, the position (wavelength) of the maximum value of the emissive changes from the short wavelength side to the long wave head side in the wavelength stage of $7.0\mu\text{m}\sim 9.0\mu\text{m}$. In other words, maximum value shows a tendency to change from $7.0\mu\text{m}$ (acidity) to $9.0\mu\text{m}$ (super-base).
- The absorption spectrum to originate in the oscillation of Si-O appears in the wavelength range of $8.5\mu\text{m}\sim 12.0\mu\text{m}$. The wavelength that emissive is minimized, wavelength of tectosilicate, which degree of condensation of SiO_4 is high, is short(the neighborhood of $9.0\mu\text{m}$), and wavelength of solosilicate and nesosilicate, which the degree of condensation are low, get long as for. (nearly $11.5\mu\text{m}$)
- Only tectosilicate salt shows absorption spectrum in the wavelength range of $12.0\mu\text{m}\sim 15.0\mu\text{m}$, and other silicate minerals don't show absorption.

Fig. 3.7

Transparent spectral curve in thermal infrared wavelength range of typical rock

Number 10 - 14 is the observation bands of ASTER.



3.3 List of ASTER imagery

| No. | Mineral Deposit Site | Volume | Observation Date | Granule ID |
|-----|------------------------------------|--------|------------------|-----------------------------------|
| 1 | Sfariat | 1 | 13/10/2002 | AST3A-1 021013 113053 021102 0453 |
| 2 | Zouerate (Kadia & Tiris) | 1 | 23/10/2000 | AST3A-1 001023 114355 031217 1168 |
| 3 | | 2 | 23/10/2000 | AST3A-1 001023 114404 031217 1168 |
| 4 | | 3 | 08/09/2001 | AST3A-1 010908 113645 031217 1169 |
| 5 | | 4 | 08/09/2001 | AST3A-1 010908 113654 031217 1181 |
| 6 | Tasiast (Tasiast & Tijirit) | 1 | 23/07/2000 | AST3A-1 000723 111945 041006 0911 |
| 7 | | 2 | 19/09/2000 | AST3A-1 000919 115752 031217 1170 |
| 8 | | 3 | 19/09/2000 | AST3A-1 000919 115801 031217 1171 |
| 9 | | 4 | 21/10/2000 | AST3A-1 001021 115656 031217 1185 |
| 10 | | 5 | 21/10/2000 | AST3A-1 001021 115705 031217 1182 |
| 11 | | 6 | 22/02/2002 | AST3A-1 020232 113855 020306 2189 |
| 12 | | 7 | 22/02/2002 | AST3A-1 020232 113846 020306 2188 |
| 13 | Akjoujt (Taburinkout & Inchiri) | 1 | 01/12/2000 | AST3A-1 001201 114958 031217 1172 |
| 14 | | 2 | 11/12/2001 | AST3A-1 011211 114657 031217 1172 |
| 15 | Kadiar (Kadiar & Indice78) | 1 | 07/10/2000 | AST3A-1 001007 114546 031217 1174 |
| 16 | | 2 | 01/11/2003 | AST3A-1 031101 113145 031217 1183 |
| 17 | | 3 | 07/10/2000 | AST3A-1 001007 114555 031217 1186 |
| 18 | | 4 | 01/11/2003 | AST3A-1 031101 113154 031217 1175 |
| 19 | Diaguili (Diaguili & Guidimaka) | 1 | 30/09/2000 | AST3A-1 000930 114009 031217 1176 |
| 20 | | 2 | 23/11/2002 | AST3A-1 021123 112722 031217 1177 |
| 21 | | 3 | | |
| 22 | Jreida-Lemsid | 1 | 03/09/2000 | AST3A-1 000903 115845 031217 1178 |
| 23 | | 1 | | |

3.4 List of LANDSAT ETM

| No. | PATH | ROW | Observation date | Mineral deposit site |
|-----|------|-----|------------------|---------------------------------|
| 1 | 199 | 43 | 27/04/2003 | |
| 2 | 200 | 42 | 04/05/2003 | |
| 3 | 200 | 43 | 04/05/2003 | |
| 4 | 201 | 42 | 09/04/2003 | |
| 5 | 201 | 43 | 09/04/2003 | |
| 6 | 202 | 42 | 16/04/2003 | |
| 7 | 202 | 43 | 16/04/2003 | |
| 8 | 202 | 44 | 16/04/2003 | |
| 9 | 202 | 49 | 27/02/2003 | Diaguili (Guidimaka & Diaguili) |
| 10 | 202 | 50 | 27/02/2003 | Diaguili (Guidimaka & Diaguili) |
| 11 | 203 | 42 | 06/03/2003 | |
| 12 | 203 | 43 | 06/03/2003 | Sfariat |
| 13 | 203 | 44 | 06/03/2003 | Kedia (kedia & Tiris) |
| 14 | 203 | 45 | 06/03/2003 | Kediar (kedia & Tiris) |
| 15 | 203 | 46 | 06/03/2003 | |
| 16 | 203 | 47 | 06/03/2003 | |
| 17 | 203 | 48 | 06/03/2003 | Kadiar (Kadiar & Indice78) |
| 18 | 203 | 49 | 06/03/2003 | Kadiar (Kadiar & Indice78) |
| 19 | 204 | 44 | 14/04/2003 | |
| 20 | 204 | 45 | 14/04/2003 | |
| 21 | 204 | 46 | 14/04/2003 | Akjoujt (Inchiri & Taburinkout) |
| 22 | 204 | 47 | 14/04/2003 | Akjoujt (Inchiri & Taburinkout) |
| 23 | 204 | 48 | 14/04/2003 | |
| 24 | 204 | 49 | 13/03/2003 | |
| 25 | 205 | 45 | 05/04/2003 | |
| 26 | 205 | 46 | 05/04/2003 | Tasiast (Tasiast & Tijirit) |
| 27 | 205 | 47 | 05/04/2003 | Tasiast (Tasiast & Tijirit) |
| 28 | 205 | 48 | 05/04/2003 | |
| 29 | 206 | 45 | 28/04/2003 | |
| 30 | 206 | 46 | 28/04/2003 | |

3.5 List of Topographical Map (1:200,000)

| No. | Map No. | Name of Map | No. | Map No. | Name of Map | No. | Map No. | Name of Map |
|-----|---------|-----------------|-----|---------|-----------------|-----|---------|-------------|
| 4 | 2510 | Bel guerdan | 54 | 1910 | Adofer el Abiod | 80 | 1706 | Nkhaile |
| 5 | 2509 | Ain Ben Till | 55 | 1909 | Hoflat Sardoun | 81 | 1705 | Zouina |
| 10 | 2411 | Tourassin | 56 | 1908 | Abolog | 82 | 1616 | Saint-Louis |
| 11 | 2410 | Glelbat | 57 | 1907 | Oumm Ahmar | 83 | 1615 | Dagana |
| 12 | 2409 | Tmelimichat | 58 | 1906 | Kratil | 84 | 1614 | Podor |
| 16 | 2312 | Oumn Dfeiret | 59 | 1905 | El Felje | 85 | 1613 | Kaedi |
| 17 | 2311 | Oumn Rouelssine | 60 | 1815 | Nouakchott | 86 | 1612 | Mbout |
| 18 | 2310 | Zednes | 61 | 1814 | Aguilal-Fal | 87 | 1611 | kiffa |
| 19 | 2309 | Rhall Amane | 62 | 1813 | Bir-Allah | 88 | 1610 | Tintane |
| 23 | 2212 | Fderik | 63 | 1812 | Ksar el Barka | 89 | 1609 | Nema |
| 24 | 2211 | Tourine | 64 | 1811 | Tidjikja | 90 | 1608 | Timbedgha |
| 25 | 2210 | Tenoumer | 65 | 1810 | Ganeb | 91 | 1607 | Hassi Touli |
| 26 | 2209 | Aguelt | 66 | 1809 | Tichit | 92 | 1606 | Niout |
| 30 | 2112 | Ohar | 67 | 1808 | Aratane | 93 | 1605 | Selibabi |
| 31 | 2111 | Guelb er Richat | 68 | 1807 | Kedama | 94 | 1513 | Matam |
| 37 | 2016 | Nouadhibou | 69 | 1806 | Aklet-Awana | 95 | 1512 | Selimane |
| 38 | 2015 | Chami | 70 | 1805 | Mgata Tauria | 96 | 1511 | Kankossa |
| 39 | 2014 | Ahmeyine | 71 | 1715 | Nimjat | 97 | 1510 | Yelomane |
| 40 | 2013 | Atar | 72 | 1714 | Boutilimit | 98 | 1509 | Nioro |
| 41 | 2012 | Chinguetti | 73 | 1713 | Aleg | 99 | 1508 | Balle |
| 42 | 2011 | Ouadane | 74 | 1712 | Moudjeria | 100 | 1507 | Nara |
| 49 | 1915 | Nouamghar | 75 | 1711 | Boumdeid | 101 | 1506 | Sege |
| 50 | 1914 | Akjoujt | 76 | 1710 | Tamchekket | 102 | 1505 | Nampla |
| 51 | 1913 | El gleltat | 77 | 1709 | Bou Derga | 103 | 1412 | Bakel |
| 52 | 1912 | Far aoun | 78 | 1708 | Ouftene | 104 | 1411 | kayes |
| 53 | 1911 | El Moinan | 79 | 1707 | Oualata | | | |